On the Achievable Spectral Efficiency of Non-Orthogonal Frequency Division Multiplexing

Yuto Hama, *Member, IEEE,* and Hideki Ochiai, *Fellow, IEEE*

Abstract— We investigate the spectral efficiency of non-orthogonal frequency division multiplexing (NOFDM). NOFDM is regarded as a frequency-domain faster-than-Nyquist (FTN) signaling with block transmission, where each subcarrier is compressed in the frequency domain by utilizing the discrete fractional Fourier transform (DFRFT). Since pulse shaping filters are not employed, the effective bandwidth of the NOFDM signal should take into account the resulting out-of-band (OOB) radiation. Therefore, we derive a closed-form expression for the power spectral density (PSD) of the NOFDM signal with windowing for OOB reduction. Through numerical comparison, it is shown that NOFDM outperforms OFDM in view of the effective signal bandwidth if they are compared under the same number of subcarriers. On the other hand, by the capacity analysis based on the asymptotic spectral efficiency with a large number of subcarriers, we elucidate that NOFDM may not outperform OFDM from an information-theoretic perspective.

Index Terms— Capacity, discrete Fourier transform (DFT), discrete fractional Fourier transform (DFRFT), faster-than-Nyquist (FTN) signaling, non-orthogonal frequency division multiplexing (NOFDM), orthogonal frequency division multiplexing (OFDM), spectral efficiency.

I. INTRODUCTION

A drastic enhancement of spectral efficiency is urgently required in future wireless communications such as the sixth generation mobile communications standard (6G) [1]. In contrast, the spectral efficiency close to the Shannon limit has been achieved by state-of-the-art physical layer techniques. In modern high speed wireless communication systems such as cellular networks and wireless LAN, the block transmission scheme based on orthogonal frequency division multiplexing (OFDM) has been a *de-facto* standard, partly due to its efficient implementation based on the fast Fourier transform (FFT).

In order to enhance the utilization of limited frequency resources, several non-orthogonal multi-carrier-based techniques have been proposed, such as non-orthogonal frequency division multiplexing (NOFDM) (i.e., non-orthogonal counterpart of OFDM) [2] and spectrally efficient frequency division multiplexing (SEFDM) [3]. These schemes are based on frequency division multiplexing (FDM) with non-orthogonal subcarriers, where the adjacent subcarriers are allocated with a smaller spacing compared to OFDM [4].

The authors are with the Department of Electrical and Computer Engineering, Yokohama National University, Yokohama, Japan. (email: yuto.hama@ieee.org; hideki@ynu.ac.jp) *(Corresponding author: Yuto Hama)*

Nearly five decades ago, faster-than-Nyquist (FTN) signaling was proposed for single-carrier transmission with pulse shaping filters, where each symbol is transmitted at *faster than* the Nyquist rate by intentionally violating the Nyquist criterion [5]. FTN signaling compresses adjacent orthogonal resources in the time domain, whereas NOFDM performs that in the frequency domain. Therefore, NOFDM has also been regarded as a variant of FTN signaling [6]. Furthermore, FTN can be simultaneously implemented in the time and frequency domain, and this approach is called multiple-carrier FTN (MC-FTN) [7]. In this paper, these non-orthogonal resource allocation approaches performed in the time-frequency domain are collectively referred to as FTN.

The major challenge of FTN signaling is how to deal with the interference among non-orthogonal resources, i.e., inter-symbol interference (ISI) in the time-domain FTN (TD-FTN) and inter-carrier interference (ICI) in the frequency-domain FTN (FD-FTN). Furthermore, the amount of ISI and ICI depends on the type of filters employed [8]. Therefore, in the previous studies, the achievable performance of FTN signaling with a variety of pulse shaping filters has been investigated from an information-theoretic perspective [9–12]. In practice, the root raised cosine (RRC) filter is employed for single-carrier transmission with pulse shaping. In this context, FTN signaling achieves higher capacity compared to the classical Nyquist transmission with the same RRC filter except for the case without roll-off, i.e., the ideal rectangular filter [13]. This result also holds for FD-FTN employing RRC filtering [14, 15] based on filter bank multiple carrier (FBMC). In addition, MC-FTN with RRC and Gaussian filters achieves higher capacity compared to the Nyquist transmission with the same pulse shaping filters [16].

The potential advantage of FTN signaling over the Nyquist schemes has been analyzed in terms of capacity [13]. The case for FD-FTN signaling with RRC filters has been investigated in [15]. It is important to note that the conventional analysis for the achievable spectral efficiency of FTN signaling is based on the excess bandwidth introduced by the pulse shaping filter. In practice, however, pulse shaping filters are not employed in most existing broadband wireless communication standards, such as cellular networks (4G and 5G) and wireless LAN, since they adopt block transmission based on OFDM signaling [6]. Therefore, the above-mentioned analysis is not applicable to these block transmission systems since the spectrum is controlled by windowing rather than filtering [17]. Nevertheless, to the best of the authors' knowledge, the information-theoretic analysis of the FTN signaling with block transmission over the conventional OFDM signal has not been well investigated.

Motivated by the above fact, in this work, we focus on *FTN signaling with block transmission*, which corresponds to FD-FTN of OFDM, and we refer to this simply as *NOFDM*[1]. NOFDM can be efficiently implemented by discrete fractional Fourier transform (DFRFT) instead of discrete Fourier transform (DFT) in OFDM systems [3]. Since pulse shaping filters are not employed due to the block transmission, out-of-band (OOB) radiation of the NOFDM signal degrades its spectral efficiency similar to OFDM, and thus windowing should be employed at the transmitter [17]. Therefore, we evaluate the spectral efficiency of the NOFDM signal in terms of the effective bandwidth determined based on its power spectral density (PSD) by taking the effect of windowing into account. To this end, we derive the closed-form expression of the PSD for the NOFDM signal and analyze the effective signal bandwidth. Furthermore, we develop a capacity of the NOFDM signal as an asymptotic spectral efficiency with a large number of subcarriers, based on which we conclude that OFDM (or orthogonal subcarrier allocation) is in fact the optimal form of NOFDM. The primary contributions of this paper are summarized as follows:

- We analyze the spectral efficiency of FTN signaling with practical block transmission in terms of the effective signal bandwidth achieved by windowing.
- The closed-form PSD expressions of the NOFDM signal are derived for rectangular and raised-cosine windows, based on which the spectral efficiency of NOFDM system is derived by utilizing the eigenvalue decomposition (EVD) of the equivalent channel matrix of NOFDM.
- We demonstrate that NOFDM may outperform OFDM in terms of spectral efficiency in view of the effective bandwidth if they are compared under the same number of subcarriers, but we also show that its benefit is limited to the case with a small number of subcarriers.
- We analyze the capacity of the NOFDM signal derived from the asymptotic behavior of the spectral efficiency with a large number of subcarriers, and show that OFDM is the optimal form of NOFDM.

This paper is organized as follows. In Section II, we describe the system model of the NOFDM signal. Section III focuses on the effective bandwidth of the NOFDM signal based on the PSD derived in closed-form. Theoretical analysis of NOFDM is given in Section IV, where the spectral efficiency and capacity are investigated and compared with OFDM. Finally, Section V concludes this work.

II. SYSTEM MODEL

In this section, we describe the system model of FTN signaling with block transmission using DFRFT. For the purpose of the mathematical analysis presented later, we introduce the system in a framework of the precoded NOFDM signal [18], and its block diagram is shown in Fig. 1. We note that the classical OFDM corresponds to the special case of NOFDM.

---

[1]As in [15], the term *NOFDM* is also used as an alternative to *FD-FTN of FBMC*. Strictly speaking, NOFDM should be interpreted as an *FD-FTN extension of the conventional OFDM*, which will be adopted throughout this paper.
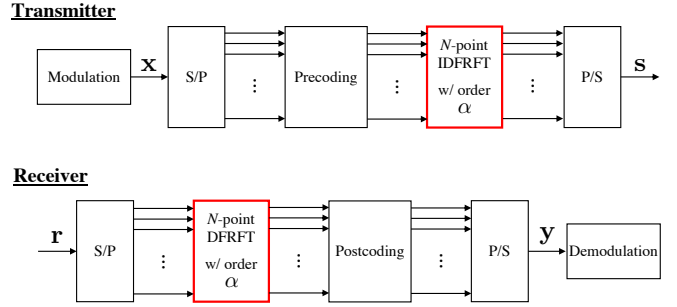
Transmitter

Receiver

Fig. 1. A block diagram of the NOFDM transmitter and receiver with the compression factor α.

Throughout this work, we focus on the fundamental performance of the NOFDM signal over an additive white Gaussian noise (AWGN) channel. Thus, the insertion of the cyclic prefix (CP) that compensates for the ISI caused by multi-path fading is not considered.

A. Discrete Fractional Fourier Transform

DFRFT is a linear transform similar to DFT, and the kth output sample of N-point DFRFT with the input $\mathbf{b} = [b_0, b_1, \cdots, b_{N-1}] \in \mathbb{C}^N$ is defined as [19]

$$B_k = \frac{1}{\sqrt{N}} \sum_{n=0}^{N-1} b_n e^{-j2\pi kna/N}, \tag{1}$$

where $a \in \mathbb{R}$ denotes the order of DFRFT. It is obvious from (1) that DFRFT is a generalization of DFT as they coincide when $a = 1$. Therefore, DFRFT can also be implemented efficiently with its complexity order $\mathcal{O}(N \log N)$ [20].

We define the DFRFT matrix with the order a and size N denoted by $\mathbf{F}_{N,a} \in \mathbb{C}^{N \times N}$ as

$$\mathbf{F}_{N,a} \triangleq$$

$$\frac{1}{\sqrt{N}} \begin{bmatrix} \omega^{a(0 \cdot 0)} & \cdots & \omega^{a(0 \cdot n)} & \cdots & \omega^{a(0 \cdot (N-1))} \\ \vdots & \ddots & \vdots & \ddots & \vdots \\ \omega^{a(k \cdot 0)} & \cdots & \omega^{a(k \cdot n)} & \cdots & \omega^{a(k \cdot (N-1))} \\ \vdots & \ddots & \vdots & \ddots & \vdots \\ \omega^{a((N-1) \cdot 0)} & \cdots & \omega^{a((N-1) \cdot n)} & \cdots & \omega^{a((N-1)(N-1))} \end{bmatrix}, \tag{2}$$

where $\omega \triangleq e^{-j2\pi/N}$. The inverse DFRFT (IDFRFT) is defined by changing the sign of the DFRFT order [21], and the IDFRFT matrix is given by $\mathbf{F}_{N,-a} = \mathbf{F}_{N,a}^{\mathrm{H}} \in \mathbb{C}^{N \times N}$ with $\mathbf{X}^{\mathrm{H}}$ representing Hermitian transpose of a matrix $\mathbf{X}$. Since the DFT and IDFT matrices correspond to the special cases of the DFRFT and IDFRFT matrices with $a = 1$, we define their shorthand notations as $\mathbf{F}_N \triangleq \mathbf{F}_{N,1}$ and $\mathbf{F}_N^{-1} \triangleq \mathbf{F}_N^{\mathrm{H}} = (\mathbf{F}_{N,1})^{\mathrm{H}}$, respectively.

B. Transmitter

In this subsection, we describe the NOFDM transmitter. Its signal processing is regarded as a generalization of the conventional OFDM, and they can be extended by generalizing DFT in OFDM to DFRFT as illustrated in Fig. 1.

We first consider the conventional OFDM signal with the symbol period T and N subcarriers. The frequency interval between the adjacent subcarriers, commonly referred to as the *subcarrier spacing (SCS)*, is given by

$$\Delta f = \frac{1}{T}, \tag{3}$$

and the orthogonality among subcarriers is guaranteed in OFDM. As a result, N data symbols are transmitted by the OFDM signal with N subcarriers during the symbol period T. Hence, the rate per each data symbol corresponds to the Nyquist interval, which is given by

$$\Delta t = \frac{T}{N}. \tag{4}$$

The sampling frequency is then expressed as

$$f_s \triangleq \frac{1}{\Delta t} = \frac{N}{T}, \tag{5}$$

whereas the corresponding Nyquist frequency is defined as

$$f_n \triangleq \frac{f_s}{2} = \frac{1}{2\Delta t} = \frac{N}{2T}. \tag{6}$$

On the other hand, the *SCS of NOFDM* is adjusted by introducing the *compression factor* denoted by $\alpha = (0, 1] \in \mathbb{R}$ as

$$\alpha \Delta f = \frac{\alpha}{T}. \tag{7}$$

Let $\mathbf{x} = [x_0, x_1, \cdots, x_{N-1}]^T \in \mathbb{C}^{N \times 1}$ denote the data symbol vector with $x_n \in \mathbb{C}$ representing the nth complex data symbol. For information-theoretic analysis, it is assumed to be an independent and identically distributed (i.i.d.) complex Gaussian random variable with the average symbol power E_s, i.e., $x_n \sim \mathcal{CN}(0, E_s)$. Thus, its covariance matrix is given by $E\{\mathbf{xx}^H\} = E_s \mathbf{I}_N$ with $\mathbf{I}_N$ representing the identity matrix of size N. The transmitted signal of NOFDM with N subcarriers is expressed as

$$s(t) = \frac{1}{\sqrt{N}} \sum_{n=0}^{N-1} x_n e^{j2\pi n\alpha \Delta f t} = \frac{1}{\sqrt{N}} \sum_{n=0}^{N-1} x_n e^{j2\pi n t\alpha/T}, \tag{8}$$

where the symbol period of NOFDM remains the same as that of OFDM, i.e., T.

From (8), the average transmission power of the NOFDM signal is calculated by

$$\frac{1}{T} \int_0^T E\left\{|s(t)|^2\right\} dt = \frac{1}{T} \int_0^T E\{s(t)s^*(t)\} dt$$
$$= \frac{1}{NT} \int_0^T E\left\{\left(\sum_{n=0}^{N-1} x_n e^{j2\pi nt\alpha/T}\right)\left(\sum_{m=0}^{N-1} x_m^* e^{-j2\pi mt\alpha/T}\right)\right\} dt$$
$$= \frac{1}{NT} \sum_{n=0}^{N-1} \sum_{m=0}^{N-1} E\{x_n x_m^*\} \int_0^T e^{j2\pi(n-m)t\alpha/T} dt$$
$$= \frac{1}{NT} \sum_{n=0}^{N-1} E\{x_n x_n^*\} \int_0^T e^0 dt$$
$$= E_s, \tag{9}$$

where by assumption $E\{x_n x_m^*\}$ takes E_s when $n = m$ and 0 otherwise. Hence, the transmission power of the NOFDM signal in (8) does not depend on the compression factor α.

We now consider the baseband symbol representation of (8). In the NOFDM signal, data symbols with N subcarriers are transmitted with the symbol interval of T regardless of the compression factor α. Hence, the rate per each data symbol corresponds to the Nyquist interval of (4). As a result, the sampling at the receiver is performed in the same principle as OFDM. Thus, the kth element of the discrete-time baseband signal discretized with the Nyquist interval of $\Delta t = T/N$ is expressed as

$$s_k \triangleq s(k\Delta t) = \frac{1}{\sqrt{N}} \sum_{n=0}^{N-1} x_n e^{j2\pi kn\alpha/N},$$
$$k \in \{0, 1, \cdots, N-1\}. \tag{10}$$

From (1) and (10), the baseband symbol of the NOFDM signal with the compression factor α is generated by IDFRFT operation with the order of $a = \alpha$ [22]. The transmitted symbol vector $\mathbf{s} = [s_0, s_1, \cdots, s_{N-1}]^T \in \mathbb{C}^{N \times 1}$ of NOFDM with linear precoding is expressed as

$$\mathbf{s} = \mathbf{F}_{N,\alpha}^H \mathbf{Px} \triangleq \mathbf{F}_{N,\alpha}^H \tilde{\mathbf{x}}, \tag{11}$$

where $\mathbf{P} \in \mathbb{C}^{N \times N}$ denotes the precoding matrix and $\tilde{\mathbf{x}} \triangleq \mathbf{Px} = [\tilde{x}_0, \tilde{x}_1, \cdots, \tilde{x}_{N-1}]^T \in \mathbb{C}^{N \times 1}$ represents the precoded data symbol vector.

C. Receiver

The received signal over an AWGN channel is expressed as

$$r(t) = s(t) + n(t), \tag{12}$$

where $n(t)$ is the AWGN term. The receiver first samples the received signal with the Nyquist interval $\Delta t = T/N$, which is matched with the sampling rate of the baseband symbol at the transmitter. The kth sample of the received baseband signal is given by

$$r_k \triangleq r(k\Delta t) = s(k\Delta t) + n(k\Delta t)$$
$$= \underbrace{\frac{1}{\sqrt{N}} \sum_{n=0}^{N-1} x_n e^{j2\pi kn\alpha/N}}_{s_k} + n_k, \quad k \in \{0, 1, \cdots, N-1\}, \tag{13}$$

where $n_k \triangleq n(k\Delta t)$ represents the kth noise sample with zero mean and complex variance of N_0, i.e., $n_k \sim \mathcal{CN}(0, N_0)$.

The received symbol vector $\mathbf{r} = [r_0, r_1, \cdots, r_{N-1}]^T \in \mathbb{C}^{N \times 1}$ is expressed as

$$\mathbf{r} = \mathbf{s} + \mathbf{n}, \tag{14}$$

where $\mathbf{n} = [n_0, n_1, \cdots, n_{N-1}]^T \in \mathbb{C}^{N \times 1}$ is the AWGN vector. Therefore, from (9), the received signal-to-noise power ratio (SNR) denoted by γ_s is defined as

$$\gamma_s \triangleq \frac{E\left\{|s_k|^2\right\}}{E\left\{|n_k|^2\right\}} = \frac{E_s}{N_0}, \tag{15}$$

which does not depend on the compression factor α either.

Similar to the conventional precoded OFDM signal, such as DFT-precoded OFDM [23], the receiver employs the post-coding after NOFDM demodulation performed by DFRFT operation. Let $\mathbf{W} \in \mathbb{C}^{N \times N}$ denote the postcoding matrix. The received symbol vector of the NOFDM signal after DFRFT operation and postcoding is expressed as

$$\begin{aligned} \mathbf{y} &= \mathbf{W}\mathbf{F}_{N,\alpha}\mathbf{r} = \mathbf{W}\mathbf{F}_{N,\alpha}\left(\mathbf{s} + \mathbf{n}\right) \\ &= \mathbf{W}\mathbf{H}_{N,\alpha}\mathbf{P}\mathbf{x} + \mathbf{W}\mathbf{F}_{N,\alpha}\mathbf{n}, \end{aligned} \tag{16}$$

where the equivalent channel matrix of NOFDM with the compression factor α and N subcarriers, referred to as the *NOFDM matrix*, is defined as

$$\mathbf{H}_{N,\alpha} \triangleq \mathbf{F}_{N,\alpha}\mathbf{F}_{N,\alpha}^{\mathrm{H}}. \tag{17}$$

The (k, n) element of the NOFDM matrix with $k, n \in \{0, 1, \cdots, N-1\}$, denoted by $\mathbf{H}_{N,\alpha}[k, n]$, is calculated as

$$\begin{aligned} \mathbf{H}_{N,\alpha}\left[k, n\right] &= \sum_{i=0}^{N-1} \mathbf{F}_{N,\alpha}\left[k, i\right] \mathbf{F}_{N,\alpha}^{\mathrm{H}}\left[i, n\right] \\ &= \sum_{i=0}^{N-1} \left(\frac{1}{\sqrt{N}} e^{2\pi ki\alpha/N} \cdot \frac{1}{\sqrt{N}} e^{-2\pi in\alpha/N} \right) \\ &= \frac{1 - e^{j2\pi\alpha(k-n)}}{N\left\{1 - e^{j2\pi\alpha(k-n)/N}\right\}} \\ &= e^{j\pi\alpha(k-n)(1-\frac{1}{N})} \frac{\sin\left\{\pi\alpha(k-n)\right\}}{N\sin\left\{\frac{\pi}{N}\alpha(k-n)\right\}}. \end{aligned} \tag{18}$$

We observe that setting $\alpha = 1$ (for OFDM), the NOFDM matrix reduces to the identity matrix with size N as

$$\mathbf{H}_{N,1} = \mathbf{F}_N\mathbf{F}_N^{\mathrm{H}} = \mathbf{I}_N. \tag{19}$$

D. EVD Precoding

In order to evaluate the spectral efficiency, we introduce the eigenvalue decomposition (EVD) precoding scheme for the NOFDM signal [15, 18].

Let λ_k denote the kth eigenvalue of the NOFDM matrix, and all the eigenvalues are assumed to be sorted in descending order with respect to the index k. Since the NOFDM matrix $\mathbf{H}_{N,\alpha}$ is Hermitian, i.e., $\left(\mathbf{H}_{N,\alpha}\right)^{\mathrm{H}} = \left(\mathbf{F}_{N,\alpha}\mathbf{F}_{N,\alpha}^{\mathrm{H}}\right)^{\mathrm{H}} = \mathbf{F}_{N,\alpha}\mathbf{F}_{N,\alpha}^{\mathrm{H}} = \mathbf{H}_{N,\alpha}$, it can be rewritten by EVD as

$$\mathbf{H}_{N,\alpha} = \mathbf{U}\boldsymbol{\Lambda}\mathbf{U}^{\mathrm{H}}, \tag{20}$$

where $\boldsymbol{\Lambda} = \mathrm{diag}\left(\lambda_0, \lambda_1, \cdots, \lambda_{N-1}\right) \in \mathbb{C}^{N \times N}$ represents the diagonal matrix composed of eigenvalues, and $\mathbf{U} = [\mathbf{u}_0, \mathbf{u}_1, \cdots, \mathbf{u}_{N-1}] \in \mathbb{C}^{N \times N}$ is the unitary matrix whose kth column $\mathbf{u}_k$ is the eigenvector corresponding to λ_k.

From (20), the precoding and postcoding matrices based on EVD are given by

$$\mathbf{P} = \mathbf{U}, \tag{21}$$

$$\mathbf{W} = \mathbf{U}^{\mathrm{H}}. \tag{22}$$

Therefore, from (16), the resulting received symbol vector of EVD-precoded NOFDM signal is expressed as

$$\begin{aligned} \mathbf{y} &= \mathbf{U}^{\mathrm{H}}\mathbf{H}_{N,\alpha}\mathbf{U}\mathbf{x} + \mathbf{U}^{\mathrm{H}}\mathbf{F}_{N,\alpha}\mathbf{n} \\ &= \boldsymbol{\Lambda}\mathbf{x} + \mathbf{z}, \end{aligned} \tag{23}$$

where $\mathbf{z} \triangleq \mathbf{U}^{\mathrm{H}}\mathbf{F}_{N,\alpha}\mathbf{n} = [z_1, z_2, \cdots, z_{N-1}]^T \in \mathbb{C}^{N \times 1}$ denotes the equivalent noise vector. Its covariance matrix is given by

$$\begin{aligned} E\left\{\mathbf{z}\mathbf{z}^{\mathrm{H}}\right\} &= E\left\{\mathbf{U}^{\mathrm{H}}\mathbf{F}_{N,\alpha}\mathbf{n}\mathbf{n}^{\mathrm{H}}\mathbf{F}_{N,\alpha}^{\mathrm{H}}\mathbf{U}\right\} = N_0\left(\mathbf{U}^{\mathrm{H}}\mathbf{H}_{N,\alpha}\mathbf{U}\right) \\ &= N_0\boldsymbol{\Lambda}. \end{aligned} \tag{24}$$

Since the precoding matrix of EVD-precoded NOFDM signal is unitary from (21), the covariance matrix of the precoded data symbol vector $\tilde{\mathbf{x}} = \mathbf{P}\mathbf{x}$ in (11) is given by

$$E\left\{\tilde{\mathbf{x}}\tilde{\mathbf{x}}^{\mathrm{H}}\right\} = E\left\{\mathbf{P}\mathbf{x}\mathbf{x}^{\mathrm{H}}\mathbf{P}^{\mathrm{H}}\right\} = E\left\{\mathbf{U}\mathbf{x}\mathbf{x}^{\mathrm{H}}\mathbf{U}^{\mathrm{H}}\right\} = E_s\mathbf{I}_N. \tag{25}$$

Therefore, EVD-precoding does not affect the resulting transmission power in (9).

III. POWER SPECTRAL DENSITY AND EFFECTIVE BANDWIDTH

The primary issue in block transmission of the NOFDM signal is that its power does not localize in the frequency domain since pulse shaping filters are not employed. It leads to high OOB radiation and degrades the spectral efficiency unless a suitable windowing is applied [17]. Motivated by this fact, we define the effective bandwidth of the NOFDM signal for a given acceptable OOB radiation value. To this end, we derive closed-form expressions of the PSD for the NOFDM signal with and without windowing. Based on this PSD property, we evaluate the bandwidth of the NOFDM signal compared to the conventional OFDM signal.

A. Power Spectral Density

We first consider the power spectrum of the continuous-time signal so as to estimate the effective bandwidth of the NOFDM signal.

The transmitted NOFDM signal with windowing is expressed as

$$s_w\left(t\right) = \sum_{\ell} s^{(\ell)}\left(t\right) g\left(t - \ell T_w\right), \tag{26}$$

where $g(t)$ is a window function, $T_w\left(\geq T\right)$ represents the total NOFDM symbol length with windowing, and $s^{(\ell)}\left(t\right)$ denotes the ℓth NOFDM symbol. By writing the nth data symbol of the ℓth NOFDM symbol as $x_n^{(\ell)}$, we have

$$s^{(\ell)}\left(t\right) = \frac{1}{\sqrt{N}} \sum_{n=0}^{N-1} x_n^{(\ell)} e^{j2\pi n\alpha\Delta ft}. \tag{27}$$

From (26), the autocorrelation function of the NOFDM signal

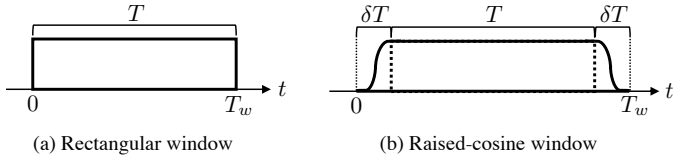(a) Rectangular window   (b) Raised-cosine window

Fig. 2. NOFDM signal structure with rectangular and raised-cosine window.

is given by

$$
\begin{aligned}
R_s\left(\tau\right) &= \lim_{T_0 \to \infty} \frac{1}{2T_0} \int_{-T_0}^{T_0} E\left\{s_w(t)s_w^*(t-\tau)\right\} dt \\
&= \frac{1}{T_w} \int_0^{T_w} \sum_{\ell=-\infty}^{\infty} \sum_{i=-\infty}^{\infty} E\left\{s^{(\ell)}(t)s^{(i)*}(t-\tau)\right\} \\
&\qquad\qquad \times g(t-\ell T_w)g^*(t-\tau-iT_w)dt \\
&= \sum_{\ell=-\infty}^{\infty} \sum_{n=0}^{N-1} \sum_{m=0}^{N-1} E\left\{\tilde{x}_n^{(\ell)}\tilde{x}_m^{(\ell)*}\right\} e^{j2\pi n\alpha\Delta f\tau} \\
&\qquad\qquad \times \frac{1}{T_w} \int_0^{T_w} g(t-\ell T_w)g^*(t-\tau-iT_w)dt \\
&= E_s \sum_{n=0}^{N-1} e^{j2\pi n\alpha\Delta f\tau} \cdot R_g\left(\tau\right),
\end{aligned}
\tag{28}
$$

where $R_g\left(\tau\right)$ represents the autocorrelation function of the window function [17]. It should be noted that EVD-precoding considered in this work does not affect the autocorrelation function since, from (25), $E\left\{\tilde{x}_n^{(\ell)}\tilde{x}_m^{(\ell)*}\right\}$ in (28) takes the same value as that without precoding[2], i.e., $E\left\{\tilde{x}_n^{(\ell)}\tilde{x}_m^{(\ell)*}\right\} = E\left\{x_n^{(\ell)}x_m^{(\ell)*}\right\}$. Thus, the PSD of the NOFDM signal is calculated as

$$
\begin{aligned}
P_s\left(f\right) &= \int_{-\infty}^{\infty} R_s\left(\tau\right) e^{-j2\pi f\tau} d\tau \\
&= E_s \sum_{k=0}^{N-1} \int_{-\infty}^{\infty} R_g\left(\tau\right) e^{-j2\pi(f-k\alpha\Delta f)\tau} d\tau \\
&= \frac{E_s}{T_w} \sum_{k=0}^{N-1} \left|G\left(f-k\alpha\Delta f\right)\right|^2,
\end{aligned}
\tag{29}
$$

where $G\left(f\right)$ is the Fourier transform (or spectrum) of $g(t)$.

Replacing the index k by $k-(N-1)/2$ leads to the symmetric PSD expressed as

$$
P_{\text{sym}}\left(f\right) = \frac{E_s}{T_w} \sum_{k=0}^{N-1} \left|G\left(f-\alpha\frac{k-\frac{N-1}{2}}{T}\right)\right|^2.
\tag{30}
$$

[2]As in the conventional precoded FTN signaling, the power allocation may improve the spectral efficiency of the NOFDM signal since the eigenvalues of the NOFDM matrix are unbalanced except when $N \to \infty$. However, it affects the resulting PSD property even under the constant transmission power condition [24] since the spectrum corresponding to the nth subcarrier depends on its allocated power, denoted by p_n, due to $E\left\{\tilde{x}_n\tilde{x}_n^*\right\} = p_n E_s$ from the covariance matrix of the precoded data symbol vector given in (25). Moreover, its optimization should be performed for each combination of the number of subcarriers N and the compression factor α. Therefore, in this work, we do not pursue the power allocation optimization but leave it as our future work.

In what follows, as a practical windowing approach, we consider the rectangular window and the raised-cosine window illustrated in Fig. 2 [25].

1) Rectangular Window: The block transmission without smooth windowing is equivalent to employing a rectangular pulse, and it is known as the rectangular window. As illustrated in Fig. 2(a), the symbol length with rectangular window T_w is identical to that of the original NOFDM signal, i.e., $T_w = T$. With the NOFDM symbol interval of T, it is given by

$$
g(t) = \begin{cases} 1, & 0 \le t < T, \\ 0, & \text{otherwise.} \end{cases}
\tag{31}
$$

Hence, its Fourier transform (or spectrum) is expressed as

$$
G(f) = \frac{1}{\sqrt{T}} \int_0^T e^{-j2\pi ft} dt = \sqrt{T} e^{-j2\pi fT} \text{sinc}(fT),
\tag{32}
$$

where

$$
\text{sinc}\left(x\right) \triangleq \frac{\sin\left(\pi x\right)}{\pi x}.
\tag{33}
$$

From (30) and (32), the symmetric PSD of the NOFDM signal with rectangular window is given by

$$
P_{\text{sym}}\left(f\right) = E_s \sum_{k=0}^{N-1} \text{sinc}^2\left[T\left(f-\alpha\frac{k-\frac{N-1}{2}}{T}\right)\right].
\tag{34}
$$

2) Raised-Cosine Window: In practical block transmission with the OFDM signal, smooth windowing is applied so as to mitigate the OOB radiation caused by the discontinuity of successive OFDM symbols. In this work, we consider the raised-cosine window (also known as Hann window) as an example [25], which is commonly employed in practical systems.

The NOFDM signal structure with raised-cosine window is illustrated in Fig. 2(b), where δT represents the transition period and δ denotes a fraction of the symbol length corresponding to the transition period. This transition period of δT is inserted at the head and tail of each NOFDM symbol. Hence, the resulting symbol length with raised-cosine window is given by $T_w = T + 2\delta T$. Its window function is expressed as [17]

$$
g(t) =
$$
$$
\begin{cases} \frac{1}{\sqrt{(4-5\delta)T_w}}\left\{1-\cos\left(\pi\frac{t}{\delta T_w}\right)\right\}, & 0 \le t < \delta T_w, \\ \frac{2}{\sqrt{(4-5\delta)T_w}}, & \delta T_w \le t < (1-\delta)T_w, \\ \frac{1}{\sqrt{(4-5\delta)T_w}}\left\{1-\cos\left(\pi\frac{T_w-t}{\delta T_w}\right)\right\}, & (1-\delta)T_w \le t < T_w, \\ 0, & \text{otherwise,} \end{cases}
\tag{35}
$$

and its Fourier transform is given by

$$
G(f) =
$$
$$
\sqrt{\frac{(1-\delta)^2 T_w}{1-\frac{5}{4}\delta}} e^{-j\pi fT_w} \frac{\cos\left(\delta T_w\pi f\right)}{1-\left(2\delta fT_w\right)^2} \text{sinc}\left(f\left(1-\delta\right)T_w\right).
\tag{36}
$$

This article has been accepted for publication in IEEE Transactions on Communications. This is the author's version which has not been fully edited and content may change prior to final publication. Citation information: DOI 10.1109/TCOMM.2023.3300328

6

Therefore, from (30) and (36), the symmetric PSD of the NOFDM signal with raised-cosine window is expressed as

$$P_{\text{sym}}(f) = E_s \frac{(1-\delta)^2}{1-\frac{5}{4}\delta} \sum_{k=0}^{N-1} \frac{\cos^2\left(\pi \frac{\delta}{1-2\delta}T\left(f-\alpha\frac{k-\frac{N-1}{2}}{T}\right)\right)}{\left[1-\left(\frac{2\delta}{1-2\delta}T\left(f-\alpha\frac{k-\frac{N-1}{2}}{T}\right)\right)^2\right]^2}$$
$$\times \text{sinc}^2\left(\frac{(1-\delta)T}{1-2\delta}\left(f-\alpha\frac{k-\frac{N-1}{2}}{T}\right)\right). \tag{37}$$

B. Effective Bandwidth

In this subsection, we discuss the bandwidth of the NOFDM signal. From (34) and (37), we observe that the bandwidth corresponding to the sidelobe spreads without limitation. In other words, the energy of the NOFDM signal does not localize in the frequency domain. Therefore, in this work, we evaluate the bandwidth of the NOFDM signal with respect to the acceptable OOB radiation value, which we define as the *effective bandwidth*.

Let p_{target} denote the target (or acceptable) PSD value for NOFDM systems. We define the *maximum frequency* f_{max} as the maximum frequency that exceeds this target PSD p_{target} derived from (34) and (37). It is expressed as

$$f_{\text{max}} \triangleq \arg \max_{f \in \mathbb{R}^+} P_{\text{sym}}(f) > p_{\text{target}}, \tag{38}$$

where $\mathbb{R}^+$ represents a set of real positive numbers. By the use of the maximum frequency f_{max}, we define the effective bandwidth of the NOFDM signal for a given PSD value p_{target} as

$$W_{\text{eff}} \triangleq 2\max\{f_n, f_{\text{max}}\} = \max\{f_s, 2f_{\text{max}}\}. \tag{39}$$

C. Spectrum of Baseband NOFDM Signal

We consider the spectrum of discrete-time NOFDM signal. Fig. 3 illustrates the spectrum of the baseband symbol of OFDM and NOFDM signals sampled at the Nyquist interval of $\Delta t = T/N$ in (10). By the sampling theorem, the spectrum of the baseband NOFDM signal should be periodic, and its period corresponds to the sampling frequency f_s. In Fig. 3, W_{main} denotes the bandwidth corresponding to the mainlobe in the NOFDM signal with the compression factor α. It is generally defined as

$$W_{\text{main}} \triangleq \Delta f + |f_{c,N-1} - f_{c,0}| = \frac{1+\alpha(N-1)}{T}, \tag{40}$$

where $f_{c,k}$ represents the central frequency of the kth subcarrier in the NOFDM signal, which is given by

$$f_{c,k} = \alpha\frac{k-\frac{N-1}{2}}{T}. \tag{41}$$

It is clear from (40) that the bandwidth of the mainlobe decreases as the compression factor α decreases. Hence, it is considered in the previous studies on FD-FTN signaling that its bandwidth can be reduced arbitrarily by compressing the subcarrier spacing [3, 15, 26]. However, this often misleads the actual spectral efficiency of FD-FTN signaling
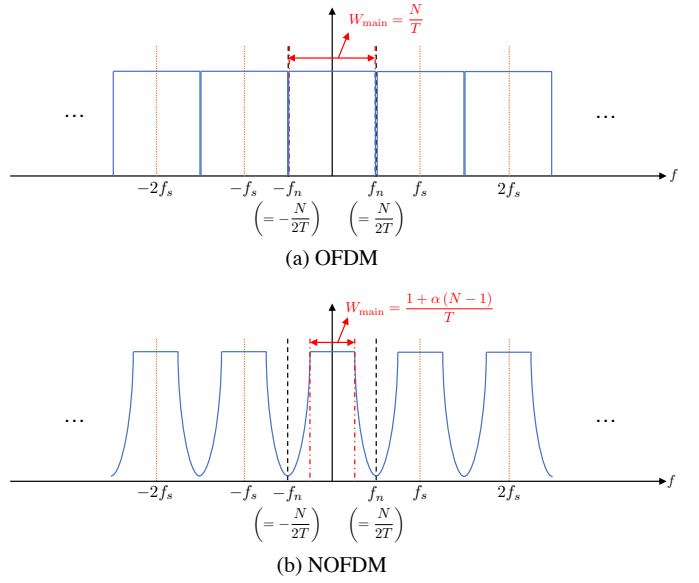

Fig. 3. The spectrum of baseband OFDM and NOFDM signals sampled at the sampling frequency of $f_s = N/T$.

since, in practice, the effect of sampling should be taken into account. In the NOFDM signal, the sampling frequency and the Nyquist frequency are given by $f_s = N/T$ in (5) and $f_n = f_s/2 = N/2T$ in (6), respectively, regardless of the compression factor α, as its baseband symbol is sampled at the Nyquist interval of $\Delta t = T/N$ so as to detect the symbols corresponding to all subcarriers. Therefore, the sampling rate is always larger than the bandwidth corresponding to the mainlobe for the NOFDM signal, i.e., $f_s \geq W_{\text{main}}$ due to the fact that $0 < \alpha \leq 1$. As a result, the spectrum of the baseband NOFDM signal with $\alpha < 1$ contains its sidelobe below the Nyquist frequency as illustrated in Fig. 3, since the sidelobe cannot be removed in the NOFDM signal due to the block transmission structure. In other words, the bandwidth of the NOFDM signal should be determined not by the compression factor α but by the sampling frequency $f_s = N/T$, and its bandwidth should never be smaller than the sampling frequency f_s since the sidelobe is still a part of the baseband signal. This fact indicates that if there exists any interference in the range of $|f| \leq f_n$, it may not be negligible, even if it falls outside the mainlobe.

In summary, the main difference between the NOFDM and OFDM signals is that the mainlobe of the NOFDM signal occupies a bandwidth smaller than that of OFDM. Therefore, it is important to note that the effective bandwidth of the NOFDM signal, according to the definition of (39), is no smaller than the sampling frequency f_s, even though its mainlobe can be made narrower by controlling α.

D. Numerical Results

Without loss of generality, we introduce the normalized frequency, denoted by $\tilde{f}$, defined as

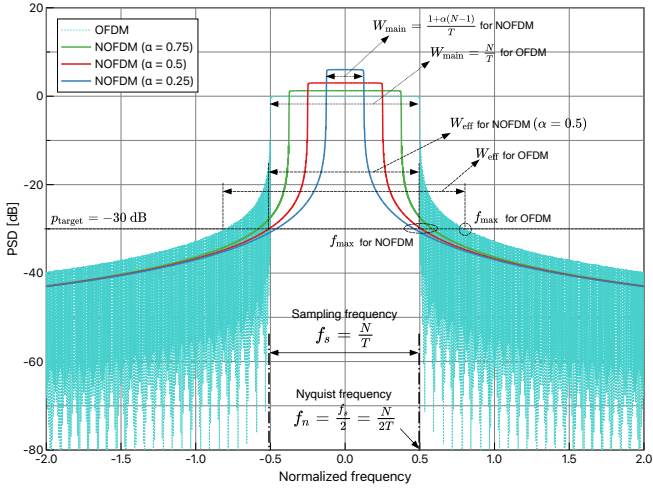$$\tilde{f} \triangleq \frac{f}{f_s}, \tag{42}$$

Fig. 4. The PSDs of OFDM ($\alpha = 1$) and NOFDM ($\alpha = 0.25, 0.5, 0.75$) signals with respect to the normalized frequency $\tilde{f}$, where the number of subcarriers is set as $N = 256$. Note that rectangular window is employed for all the signals evaluated here.
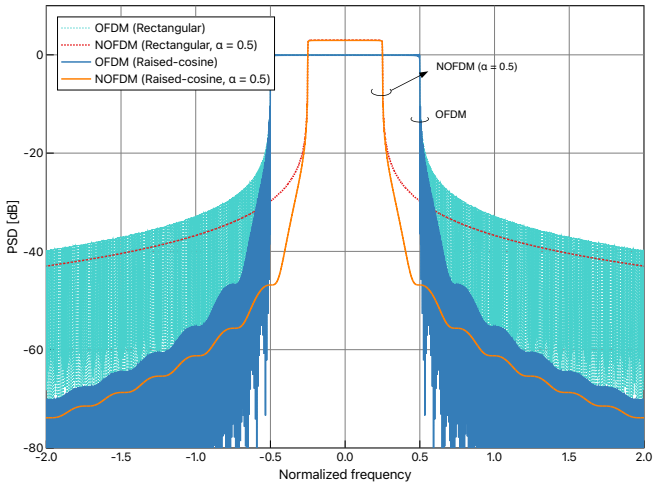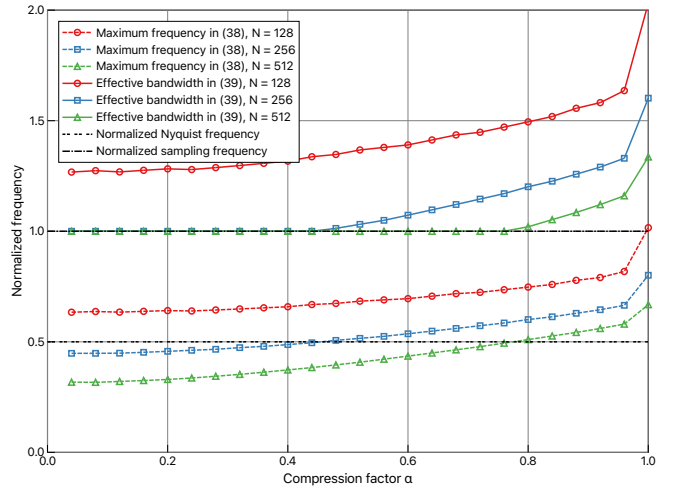

(a) Rectangular window

Fig. 5. The PSDs of OFDM ($\alpha = 1$) and NOFDM ($\alpha = 0.5$) signals with respect to the normalized frequency $\tilde{f}$, where the number of subcarriers is set as $N = 256$. The results with rectangular and raised-cosine ($\delta = 1/64$) windows are plotted by dashed and solid lines, respectively.
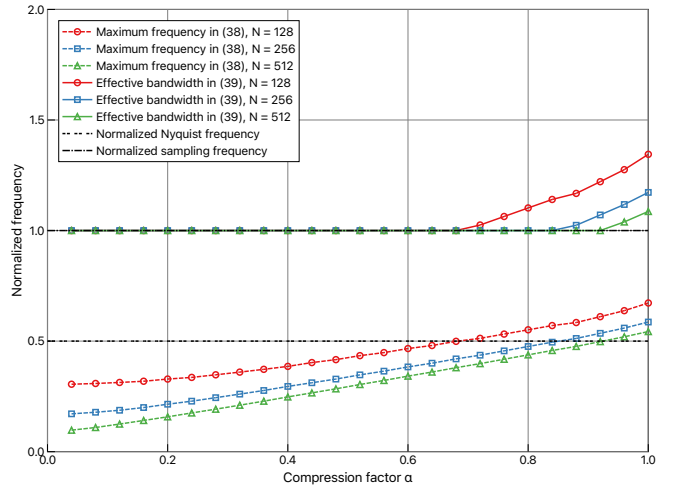

(b) Raised-cosine window ($\delta = 1/64$)

Fig. 6. The effective bandwidth and maximum frequency of the NOFDM signal with respect to the normalized frequency $\tilde{f}$, which are plotted by solid and dashed lines, respectively. The number of subcarriers is set as $N = 128, 256$, and 512.

and the corresponding normalized Nyquist frequency is introduced as

$$\tilde{f}_n \triangleq \frac{f_n}{f_s} = \frac{1}{2}. \tag{43}$$

Fig. 4 shows the PSD of the NOFDM signal with rectangular window as a function of $\tilde{f}$, where the compression factor is set as $\alpha = 0.25, 0.5, 0.75$, and 1 (OFDM), and the number of subcarriers is set as $N = 256$. From Fig. 4, the bandwidth corresponding to the mainlobe of the NOFDM signal becomes narrower by reducing the compression factor α according to (40). As a result, OOB radiation is also improved. The maximum frequency $f_{\max}$ in (38) and corresponding effective bandwidth W_{eff} in (39) are also illustrated in Fig. 4 for the target PSD of $p_{\text{target}} = -30$ dB, where we observe that $f_{\max}$ of the NOFDM signal becomes smaller than that of the OFDM

signal evaluated at the same value of p_{target}. It follows that the effective bandwidth can be improved by NOFDM. On the other hand, in the case of $\alpha = 0.25$, the maximum frequency $f_{\max}$ is smaller than the Nyquist frequency f_n for the target PSD value of $p_{\text{target}} = -30$ dB. Thus, further reduction of the compression factor α does not provide any gain in terms of the effective bandwidth W_{eff} for $p_{\text{target}} = -30$ dB.

We next evaluate the PSD of OFDM and NOFDM ($\alpha = 0.5$) signals achieved by the different windows in Fig. 5, where rectangular and raised-cosine windows are compared for $N = 256$. Here, we set the transition period of raised-cosine window as $\delta = 1/64$. As a result, raised-cosine window significantly improves OOB radiation compared to rectangular window for both OFDM and NOFDM signals.

Based on the above observation on the PSD, we evaluate the bandwidth with respect to the compression factor α. The effective bandwidth W_{eff} in (39) and maximum frequency $f_{\max}$ in (38) are plotted for the normalized frequency $\tilde{f}$ in Fig. 6, where the cases with $N = 128, 256$, and 512 are evaluated. For reference, the normalized Nyquist frequency $\tilde{f}_n$ in (43) and the normalized sampling frequency $\tilde{f}_s = f_s/f_s = 1$ are also shown in the same figure. In all cases compared in Fig. 6, the effective bandwidth achieved by raised-cosine window is smaller than that with rectangular window, since OOB radiation is improved as shown in Fig. 5. From (39), when $f_{\max} > f_n$, the effective bandwidth of the NOFDM signal is twice as large as the maximum frequency, i.e., $W_{\mathrm{eff}} = 2f_{\max}$. Since this condition is satisfied for all α in the case of rectangular window with $N = 128$, the resulting effective bandwidth can be improved as the compression factor decreases. In contrast, the maximum frequency becomes lower than the Nyquist frequency with the small compression factor for the other cases. As a result, the effective bandwidth is determined by the sampling frequency as the compression factor decreases. Therefore, the optimal compression factor may exist for each number of subcarriers N and each window.

IV. SPECTRAL EFFICIENCY AND CAPACITY

Based on the discussion on the bandwidth of the NOFDM signal in the previous section, we derive the achievable spectral efficiency and capacity based on EVD-precoding.

A. Mutual Information

From (23), the kth received symbol of EVD-precoded NOFDM signal is expressed as

$$y_k = \lambda_k x_k + z_k, \tag{44}$$

where z_k is an i.i.d. Gaussian random variable with zero mean and complex variance of $\lambda_k N_0$ from (24), i.e., $z_k \sim \mathcal{CN}(0, \lambda_k N_0)$. Therefore, the NOFDM signal with N subcarriers can be divided into N parallel complex Gaussian channels, and the equivalent SNR corresponding to the kth NOFDM channel is given by

$$\Gamma_k \triangleq \frac{E\left\{|\lambda_k x_k|^2\right\}}{E\left\{|z_k|^2\right\}} = \lambda_k \frac{E_s}{N_0} = \lambda_k \gamma_s. \tag{45}$$

The mutual information between the data symbol vector $\mathbf{x} \in \mathbb{C}^{N \times 1}$ and the received symbol vector $\mathbf{y} \in \mathbb{C}^{N \times 1}$ of the NOFDM signal in (23) is expressed as

$$I(\mathbf{x}; \mathbf{y}) = h(\mathbf{y}) - h(\mathbf{y}|\mathbf{x}) = h(\mathbf{y}) - h(\mathbf{z}), \tag{46}$$

where $h(\cdot)$ represents the differential entropy. For mathematical analysis, we assume that each data symbol x_k is an i.i.d. complex Gaussian random variable, i.e., $x_k \sim \mathcal{CN}(0, E_s)$.

Hence, the mutual information in (46) can be rewritten as

$$
\begin{aligned}
I(\mathbf{x}; \mathbf{y}) &= \sum_{k=0}^{N-1} \left[h(y_k) - h(z_k)\right] \\
&= \sum_{k=0}^{N-1} \left[\log_2\left(\pi e\left(\lambda_k^2 E_s + \lambda_k N_0\right)\right) - \log_2\left(\pi e \lambda_k N_0\right)\right] \\
&= \sum_{k=0}^{N-1} \log_2\left(1 + \lambda_k \frac{E_s}{N_0}\right) \\
&= \sum_{k=0}^{N-1} \log_2\left(1 + \Gamma_k\right) \quad \text{[bits]}.
\end{aligned}
\tag{47}
$$

Since the diagonal element of the NOFDM matrix is given by $\mathbf{H}_{N,\alpha}[k,k] = 1$ from (18), the sum of the eigenvalues is expressed as

$$\sum_{k=0}^{N-1} \lambda_k = \mathrm{tr}(\mathbf{H}_{N,\alpha}) = \sum_{k=0}^{N-1} \mathbf{H}_{N,\alpha}[k,k] = N, \tag{48}$$

where $\mathrm{tr}(\mathbf{X})$ represents the trace of a matrix $\mathbf{X}$. Therefore, from Jensen's inequality and (48), the mutual information of the NOFDM signal in (47) can be bounded as

$$I(\mathbf{x}; \mathbf{y}) \le N \log_2\left(1 + \frac{1}{N}\sum_{k=0}^{N-1}\Gamma_k\right) = N \log_2(1 + \gamma_s), \tag{49}$$

where the equality holds if and only if the compression factor is chosen as $\alpha = 1$ from (19). Therefore, NOFDM with $\alpha < 1$ is inferior to OFDM ($\alpha = 1$) in terms of mutual information.

B. Spectral Efficiency

We develop the achievable spectral efficiency of the NOFDM signal considering its PSD. The spectral efficiency of the NOFDM signal is expressed from (47) as

$$
\begin{aligned}
\eta_{\mathrm{NOFDM}}(p_{\mathrm{target}}) &\triangleq \frac{1}{TW_{\mathrm{eff}}} I(\mathbf{x}; \mathbf{y}) \\
&= \frac{1}{TW_{\mathrm{eff}}} \sum_{k=0}^{N-1} \log_2(1 + \Gamma_k) \\
&= \frac{1}{TW_{\mathrm{eff}}} \sum_{k=0}^{N-1} \log_2(1 + \lambda_k \gamma_s) \quad \text{[bits/s/Hz]},
\end{aligned}
\tag{50}
$$

where W_{eff} is the effective bandwidth of the NOFDM signal for a given target PSD value p_{target} defined in (39). In the case of raised-cosine window, the time duration T in (50) is replaced by $(1+\delta)T$ since the support of $g(t)$ in (35) is $(0, T + 2\delta T)$ and the tail part of δT overlaps with the head part of the next NOFDM symbol [17]. Hence, the rate loss by raised-cosine window is expressed as $T/(T + 2\delta T - \delta T) = 1/(1+\delta)$.

When $\alpha = 1$, since $\lambda_k = 1$ holds for all $k \in \{0, 1, \cdots, N-1\}$ from (19), the spectral efficiency of the OFDM signal is derived as

$$\eta_{\mathrm{OFDM}}(p_{\mathrm{target}}) = \frac{N}{TW_{\mathrm{eff}}} \log_2(1 + \gamma_s) \quad \text{[bits/s/Hz]}. \tag{51}$$

As demonstrated in Section III, NOFDM can be made superior to OFDM in terms of the effective bandwidth compared at the same target PSD value. Hence, there may be the case that NOFDM outperforms OFDM in terms of spectral efficiency, whereas it is not advantageous in terms of mutual information as described in the previous subsection.

C. Capacity

Finally, we investigate the asymptotic behavior of the spectral efficiency of the NOFDM signal with a large number of subcarriers. In this work, we define the *capacity* of block transmission systems as the asymptotic spectral efficiency achieved by $N \to \infty$. Since the normalized spectrum of the NOFDM signal is strictly limited to $[-\alpha/2, \alpha/2]$ (see Appendix A), the NOFDM matrix $\mathbf{H}_{N,\alpha}$ with $N \to \infty$ has only $\lceil \alpha N \rceil$ eigenvalues of $1/\alpha$, while the remaining eigenvalues approach zero [27]. From (50), the capacity of the NOFDM signal is expressed in terms of α as

$$\lim_{N \to \infty} \eta_{\text{NOFDM}}(p_{\text{target}}) = \lim_{N \to \infty} \frac{1}{TW_{\text{eff}}} \sum_{k=0}^{N-1} \log_2(1 + \lambda_k \gamma_s)$$

$$= \frac{1}{T\left(f_n \tilde{W}_{\text{inf}}\right)} \sum_{k=0}^{\lceil \alpha N \rceil - 1} \log_2\left(1 + \frac{1}{\alpha}\gamma_s\right)$$

$$= \frac{1}{N} \sum_{k=0}^{\lceil \alpha N \rceil - 1} \log_2\left(1 + \frac{\gamma_s}{\alpha}\right)$$

$$= \alpha \log_2\left(1 + \frac{\gamma_s}{\alpha}\right) \triangleq C_{\text{NOFDM}}(\alpha) \quad \text{[bits/s/Hz]}, \quad (52)$$

where $\tilde{W}_{\text{inf}} \triangleq \lim_{N \to \infty}(W_{\text{eff}}/f_n) = 1$ denotes the normalized bandwidth with rectangular window when $N \to \infty$ (see Appendix A)[3]. By substituting $\alpha = 1$ into (52), the capacity of the OFDM signal agrees with the Shannon capacity:

$$C_{\text{OFDM}} \triangleq C_{\text{NOFDM}}(1) = \log_2(1 + \gamma_s) \quad \text{[bits/s/Hz]}. \quad (53)$$

As a result, the capacity of the NOFDM signal in (52) takes the maximum value of (53) when the compression factor is $\alpha = 1$. In other words, the capacity of the OFDM signal is identical to the Shannon capacity, which cannot be achieved by the NOFDM signal with $\alpha < 1$.

D. Numerical Results

We evaluate the spectral efficiency of the NOFDM signal derived in (50) compared to that of OFDM in (51). The results with rectangular and raised-cosine ($\delta = 1/64$) window are shown in Fig. 7 evaluated for the target PSD of $p_{\text{target}} = -30$ dB at the different SNR of $\gamma_s = 0, 10$, and 20 dB, and the number of subcarriers is set to be $N = 128, 256$, and 512. As a reference, NOFDM capacity in (52) and the Shannon capacity in (53) are also plotted in the same figure. The smaller compression factor α improves the effective bandwidth

[3]When a raised-cosine window is employed, the capacity in (52) is simply degraded by the rate loss of $1/(1+\delta)$. This is due to the fact that the eigenvalues of the NOFDM matrix are not affected by windowing since the transition period of δT inserted at the head and tail of each NOFDM symbol is removed before NOFDM demodulation at the receiver.
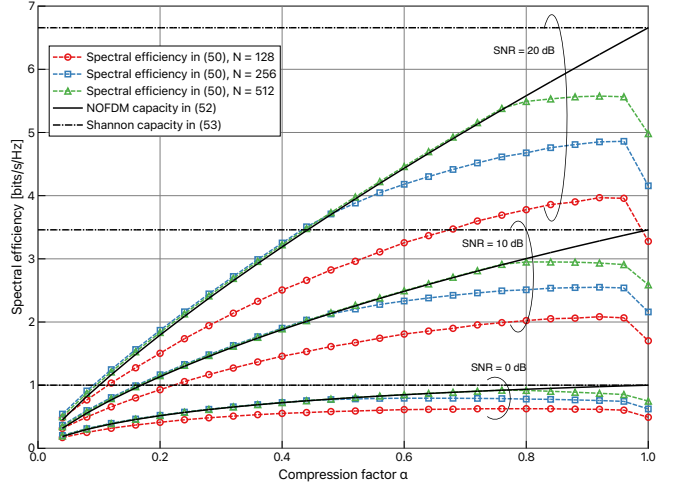
(a) Rectangular window
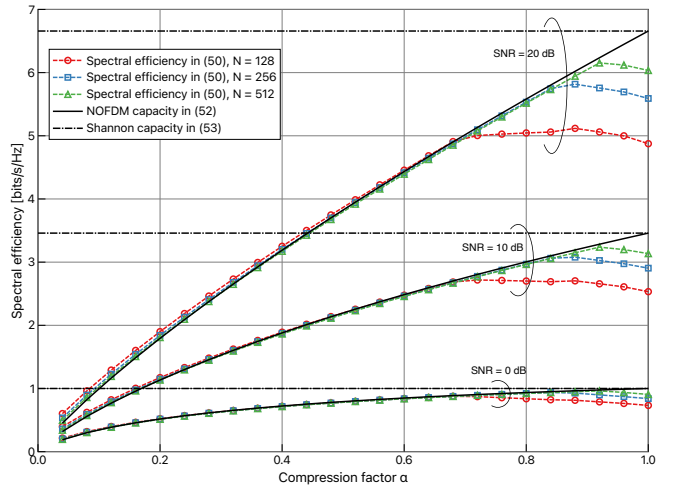
(b) Raised-cosine window

Fig. 7. The spectral efficiency of NOFDM signal with respect to the compression factor α, which is evaluated for the target PSD value $p_{\text{target}} = -30$ dB and the SNR of $\gamma_s = 0, 10$, and 20 dB. The number of subcarriers is set as $N = 128, 256$, and 512. The Shannon capacity and NOFDM capacity are also plotted by chain and solid lines, respectively.

given by (39), but it degrades the mutual information derived in (47). As a result, as observed from Fig. 7, the optimal compression factor exists for each parameter, i.e., the number of subcarriers N and the received SNR γ_s. Furthermore, the spectral efficiency achieved with raised-cosine window significantly outperforms that with rectangular window compared at the same number of subcarriers. It should be noted that the optimal compression factor also depends on the type of window employed at the transmitter. In both windowing approaches, the spectral efficiency η_{NOFDM} approaches the capacity $C_{\text{NOFDM}}(\alpha)$ as N increases according to (52).

We finally evaluate the spectral efficiency of the NOFDM signal with respect to γ_s. Fig. 8 shows the spectral efficiency and capacity of OFDM and NOFDM signals with rectangular
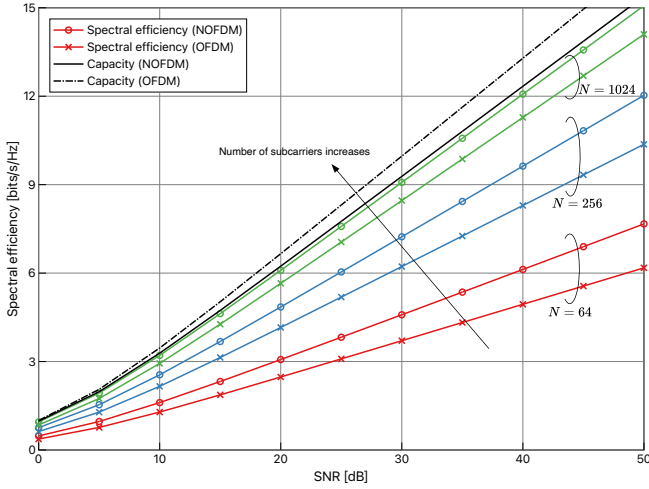
Fig. 8. The spectral efficiency of NOFDM signal ($\alpha = 0.92$) with rectangular window for the target PSD value $p_{\text{target}} = -30$ dB compared to that of OFDM signal, where the number of subcarriers is set as $N = 64, 256$, and 1024. The Shannon capacity and NOFDM capacity are also plotted.
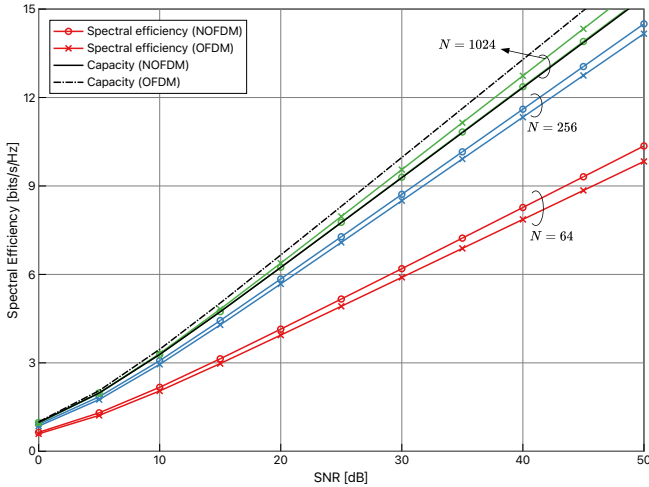

Fig. 9. The spectral efficiency of NOFDM signal ($\alpha = 0.92$) with raised-cosine window ($\delta = 1/64$) for the target PSD value $p_{\text{target}} = -30$ dB compared to that of OFDM signal, where the number of subcarriers is set as $N = 64, 256$, and 1024. The Shannon capacity and NOFDM capacity are also plotted.

window, where we set the number of subcarriers as $N = 64, 256$, and 1024. From Fig. 7, the compression factor takes different optimal values depending on the parameters. Thus, we evaluate the case with $\alpha = 0.92$ in Fig. 8 for the NOFDM signal as an example. The corresponding NOFDM capacity in (52) with $\alpha = 0.92$ is also plotted along with the Shannon capacity in (53). As the number of subcarriers N increases, the spectral efficiency of both OFDM and NOFDM improves since the OOB radiation can be decreased with the number of subcarriers. In contrast, the superiority of NOFDM over OFDM decreases as N increases. For example, the spectral efficiency of NOFDM is 1.24 times higher than that of OFDM compared with $N = 64$, but it becomes 1.07 times when $N = 1024$. Furthermore, the spectral efficiency of the NOFDM signal almost approaches its capacity when $N = 1024$, and

its further improvement may not be expected. The spectral efficiency in the case of raised-cosine window with transition period $\delta = 1/64$ is compared in Fig. 9. For all cases compared here, the spectral efficiency improves by raised-cosine window due to lower OOB radiation shown in Fig. 5. However, the advantage of NOFDM over OFDM is decreased even with $N = 64$ and 256. Furthermore, when $N = 1024$, the spectral efficiency of NOFDM with $\alpha = 0.92$ is inferior to OFDM, since OFDM achieves spectral efficiency higher than the NOFDM capacity with $\alpha = 0.92$. As a result, the optimal compression factor with raised-cosine window should be larger in this case.

In conclusion, NOFDM may have the potential advantage over OFDM in terms of spectral efficiency when they are compared with the same small number of subcarriers since non-orthogonal subcarrier allocation may reduce the effective bandwidth defined by (39) at the expense of the mutual information in (46). However, the gain achieved by non-orthogonal subcarrier allocation decreases as the number of subcarriers increases. Furthermore, OFDM ($\alpha = 1$) is superior to NOFDM with $\alpha < 1$ in terms of mutual information and capacity. In other words, OFDM is the optimal form of NOFDM from the viewpoint of information-theoretic analysis[4].

Remark: The gain of NOFDM in terms of spectral efficiency can be achieved when we consider the degradation of spectral efficiency caused by OOB radiation associated with block transmission [17]. However, the performance of NOFDM is bounded by the Shannon capacity in terms of both spectral efficiency in (50) and capacity in (52), as demonstrated in Figs. 8 and 9. Therefore, our derived results do not contradict the existing analysis for FTN signaling with pulse shaping filters [13]. As a reference, the connection between our analysis of the NOFDM signal and that of conventional FTN signaling is described in Appendix B.

V. CONCLUSION

In this work, we have investigated the achievable spectral efficiency of the NOFDM signal, which is defined as the frequency-domain FTN signal with block transmission generated by DFRFT. To this end, we have derived the closed-form expressions of the PSD for the NOFDM signal with rectangular and raised-cosine windows, and the achievable spectral efficiency has been developed by utilizing EVD precoding. As a result, NOFDM can achieve higher spectral efficiency compared to OFDM with the same number of subcarriers. On the other hand, by the capacity analysis of the NOFDM signal, we have elucidated the fact that OFDM turns out to be optimal when the number of subcarriers is large.

The optimal power allocation should be investigated for the NOFDM signal with the limited number of subcarriers and left as our future work.

---

[4]When $N \to \infty$, the SNR of each channel becomes identical since all non-zero eigenvalues take the same value of $1/\alpha$. Therefore, the non-uniform power allocation does not enhance the capacity of the NOFDM signal derived in (52).

APPENDIX

A. Asymptotic Behavior of Normalized Bandwidth for Large N

We derive the normalized bandwidth of the NOFDM signal for the cases of rectangular and raised-cosine windows, capturing the asymptotic behavior as N increases.

We first consider the rectangular window case. By substituting (42) into (34), the PSD of NOFDM signal with respect to the normalized frequency $\tilde{f}$ in (42) is expressed as

$$P_{\text{sym}}\left(\tilde{f}\right) = E_s \sum_{k=0}^{N-1} \text{sinc}^2 \left[N\left(\tilde{f} - \alpha \frac{k - \frac{N-1}{2}}{N}\right)\right]. \quad (54)$$

Furthermore, it can be bounded as

$$P_{\text{sym}}\left(\tilde{f}\right) = E_s \sum_{k=0}^{N-1} \frac{\sin^2\left[N\left(\tilde{f} - \alpha \frac{k-\frac{N-1}{2}}{N}\right)\right]}{\left[N\left(\tilde{f} - \alpha \frac{k-\frac{N-1}{2}}{N}\right)\right]^2}$$
$$\leq \sum_{k=0}^{N-1} \frac{E_s}{\left[N\left(\tilde{f} - \alpha \frac{k-\frac{N-1}{2}}{N}\right)\right]^2} \triangleq \sum_{k=0}^{N-1} c_k\left(\tilde{f}\right), \quad (55)$$

where

$$c_k\left(\tilde{f}\right) \triangleq \frac{E_s}{\left[N\left(\tilde{f} - \alpha \frac{k-\frac{N-1}{2}}{N}\right)\right]^2}. \quad (56)$$

Here, the index k takes the discrete values in the range of $0 \leq k \leq N-1$. Thus, $c_k\left(\tilde{f}\right)$ in (56) is bounded as

$$\frac{E_s}{N^2\left(\tilde{f} + \alpha \frac{N-1}{2N}\right)^2} \leq c_k\left(\tilde{f}\right) \leq \frac{E_s}{N^2\left(\tilde{f} - \alpha \frac{N-1}{2N}\right)^2}. \quad (57)$$

By taking the limit of c_k with $N \to \infty$ as

$$\frac{E_s}{\left(\tilde{f} + \frac{\alpha}{2}\right)^2} \lim_{N\to\infty} \frac{1}{N^2} \leq \lim_{N\to\infty} c_k\left(\tilde{f}\right) \leq \frac{E_s}{\left(\tilde{f} - \frac{\alpha}{2}\right)^2} \lim_{N\to\infty} \frac{1}{N^2}, \quad (58)$$

we have

$$\lim_{N\to\infty} c_k\left(\tilde{f}\right) = 0, \quad \text{for } \left|\tilde{f}\right| > \frac{\alpha}{2}. \quad (59)$$

From (54) and (59), the limit of the PSD of the NOFDM signal is expressed as

$$\lim_{N\to\infty} P_s\left(\tilde{f}\right) = 0, \quad \text{for } \left|\tilde{f}\right| > \frac{\alpha}{2}. \quad (60)$$

Hence, the *normalized* maximum frequency with $N \to \infty$ can be derived as

$$\tilde{f}_{\max} = \frac{\alpha}{2}. \quad (61)$$

Therefore, from (39) and (43), the normalized bandwidth of the NOFDM signal with $N \to \infty$ is given by

$$\tilde{W}_{\text{inf}} = 2\max\left\{\frac{f_n}{f_s}, \frac{f_{\max}}{f_s}\right\} = 2\max\left\{\tilde{f}_n, \tilde{f}_{\max}\right\}$$
$$= 2\max\left\{\frac{1}{2}, \frac{\alpha}{2}\right\} = 1. \quad (62)$$

Note that the power spectrum of the NOFDM signal with $N \to \infty$ is strictly limited to $[-\alpha/2, \alpha/2]$ due to (61), and this spectrum localization holds only for asymptotic case as $N \to \infty$.

We next consider the raised-cosine window case. By substituting (42) into (37), an upper bound on the PSD of the NOFDM signal with raised-cosine window with respect to the normalized frequency $\tilde{f}$ can be derived as

$$P_{\text{sym}}\left(\tilde{f}\right) = E_s \frac{(1-\delta)^2}{1-\frac{5}{4}\delta} \sum_{k=0}^{N-1} \frac{\cos^2\left(\pi \frac{\delta}{1-2\delta} N\left(\tilde{f} - \alpha \frac{k-\frac{N-1}{2}}{N}\right)\right)}{\left[1 - \left(\frac{2\delta}{1-2\delta} N\left(\tilde{f} - \alpha \frac{k-\frac{N-1}{2}}{N}\right)\right)^2\right]^2}$$
$$\times \text{sinc}^2\left(\frac{1-\delta}{1-2\delta} N\left(\tilde{f} - \alpha \frac{k-\frac{N-1}{2}}{N}\right)\right)$$
$$\leq \frac{(1-\delta)(1-2\delta)}{1-\frac{5}{4}\delta} \sum_{k=0}^{N-1} \frac{c_k\left(\tilde{f}\right)}{\left\{1 - \left(\frac{2\delta}{1-2\delta}\right)^2 \frac{E_s}{c_k\left(\tilde{f}\right)}\right\}^2}. \quad (63)$$

From (59) and (63), the asymptotic behavior of the PSD of the NOFDM signal with raised-cosine window satisfies (60) as well.

Therefore, the normalized bandwidth of the NOFDM signal with $N \to \infty$ agrees with (62) even with raised-cosine windowing.

B. Connection With Conventional Time-Domain FTN Signaling

Our analysis and results on the spectral efficiency of the NOFDM signal are also applicable to conventional FTN signaling with pulse shaping filters, where each symbol is compressed by a factor of τ in the time domain [5]. First, we note that our derived spectral efficiency is defined as (50) in terms of the acceptable PSD value p_{target} based on the effective bandwidth W_{eff}. Since the symbol time duration is strictly limited for the NOFDM signal by windowing, its power spectrum is unbounded. Fig. 10(a) and (b) illustrate the relationship between the time domain window and the power spectrum of the NOFDM signal with N subcarriers compressed by a factor of α. Its spectral efficiency improves as the sidelobe decreases rapidly since the effective bandwidth W_{eff} for a given acceptable OOB level can be reduced. This is achieved by compressing the subcarrier spacing by controlling α as demonstrated in Fig. 6. On the other hand, the bandwidth of the conventional FTN signaling is strictly limited by the pulse shaping filter, and thus its impulse response observed in the time domain should be unbounded. Fig. 10(c) and (d) show the signal bandwidth and time domain frame structure illustrated for a given frame transmission containing N symbols compressed by τ. Similar to the case of the NOFDM signal, the spectral efficiency of conventional time domain FTN signaling can be defined based on the effective frame duration T_{eff}, which is determined by the acceptable inter-frame interference (IFI) level as illustrated in Fig. 10(d). As a result, for a given type of frequency domain window (i.e., pulse shaping filter), reducing the symbol spacing controlled
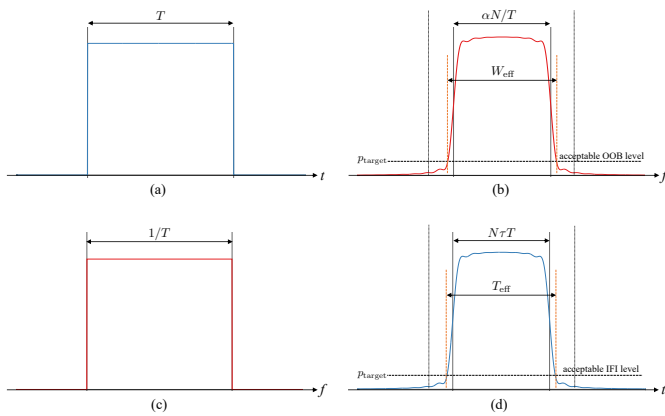
This article has been accepted for publication in IEEE Transactions on Communications. This is the author's version which has not been fully edited and content may change prior to final publication. Citation information: DOI 10.1109/TCOMM.2023.3300328

12

Fig. 10. NOFDM signal with N subcarriers compressed by a factor of α for the orthogonal frequency spacing of $1/T$: (a) time domain window and (b) power spectrum, and conventional time-domain FTN signaling with N symbols compressed by a factor of τ for the orthogonal time spacing of T: (c) power spectrum and (d) time-domain frame structure.

by τ will also improve the overall efficiency as the guard time between the successive frames (i.e., the effective frame duration T_{eff}) can be reduced. In conclusion, by switching the domains, our analysis and results are equally applicable to conventional FTN signaling with pulse shaping filters.

REFERENCES

[1] Z. Zhang *et al.*, "6G wireless networks: Vision, requirements, architecture, and key technologies," *IEEE Veh. Technol. Mag.*, vol. 14, no. 3, pp. 28–41, 2019.

[2] W. Kozek and A. F. Molisch, "Nonorthogonal pulseshapes for multicarrier communications in doubly dispersive channels," *IEEE J. Sel. Areas Commun.*, vol. 16, no. 8, pp. 1579–1589, 1998.

[3] I. Kanaras, A. Chorti, M. R. Rodrigues, and I. Darwazeh, "Spectrally efficient FDM signals: Bandwidth gain at the expense of receiver complexity," in *Proc. IEEE ICC*, Jun. 2009.

[4] M. Rodrigues and I. Darwazeh, "A spectrally efficient frequency division multiplexing based communications system," in *Proc. Int. OFDM Workshop*, Sep. 2003.

[5] J. E. Mazo, "Faster-than-Nyquist signaling," *Bell Syst. Tech. J.*, vol. 54, no. 8, pp. 1451–1462, 1975.

[6] J. Fan, S. Guo, X. Zhou, Y. Ren, G. Y. Li, and X. Chen, "Faster-than-Nyquist signaling: An overview," *IEEE Access*, vol. 5, pp. 1925–1940, 2017.

[7] F. Rusek and J. B. Anderson, "Multistream faster than Nyquist signaling," *IEEE Trans. Commun.*, vol. 57, no. 5, pp. 1329–1340, 2009.

[8] A. Modenini, F. Rusek, and G. Colavolpe, "Optimal transmit filters for ISI channels under channel shortening detection," *IEEE Trans. Commun.*, vol. 61, no. 12, pp. 4997–5005, 2013.

[9] A. D. Liveris and C. N. Georghiades, "Exploiting faster-than-Nyquist signaling," *IEEE Trans. Commun.*, vol. 51, no. 9, pp. 1502–1511, 2003.

[10] F. Rusek and J. B. Anderson, "Non binary and precoded faster than Nyquist signaling," *IEEE Trans. Commun.*, vol. 56, no. 5, pp. 808–817, 2008.

[11] D. Dasalukunte, F. Rusek, and V. Owall, "Multicarrier faster-than-Nyquist transceivers: Hardware architecture and performance analysis," *IEEE Trans. Circuits Syst. I*, vol. 58, no. 4, pp. 827–838, 2010.

[12] J. B. Anderson and F. Rusek, "Optimal side lobes under linear and faster-than-Nyquist modulation," in *Proc. IEEE ISIT*, Jun. 2007.

[13] F. Rusek and J. B. Anderson, "Constrained capacities for faster-than-Nyquist signaling," *IEEE Trans. Inf. Theory*, vol. 55, no. 2, pp. 764–775, 2009.

[14] Y. Feng, Y. Ma, Z. Li, C. Yan, and N. Wu, "Low-complexity factor graph-based iterative detection for RRC-SEFDM signals," in *Proc. WCSP*, Oct. 2018.

[15] S. Osaki, T. Ishihara, and S. Sugiura, "Eigenvalue-decomposition-precoded ultra-dense non-orthogonal frequency-division multiplexing," *IEEE Trans. Wireless Commun.*, vol. 19, no. 12, pp. 8165–8178, 2020.

[16] A. Barbieri, D. Fertonani, and G. Colavolpe, "Time-frequency packing for linear modulations: spectral efficiency and practical detection schemes," *IEEE Trans. Commun.*, vol. 57, no. 10, pp. 2951–2959, 2009.

[17] H. Ochiai, "On spectral efficiency of OFDM signals based on windowing," *IEICE Trans. Fundamentals*, vol. E106-A, no. 5, 2023. [Online]. Available: https://www.jstage.jst.go.jp/article/transfun/E106.A/5/E106.A_2022WBI0002/_article

[18] S. Isam and I. Darwazeh, "Precoded spectrally efficient FDM system," in *Proc. IEEE PIMRC*, Sep. 2010.

[19] D. H. Bailey and P. N. Swarztrauber, "The fractional Fourier transform and applications," *SIAM review*, vol. 33, no. 3, pp. 389–404, 1991.

[20] H. M. Ozaktas, O. Arikan, M. A. Kutay, and G. Bozdagt, "Digital computation of the fractional Fourier transform," *IEEE Trans. Signal Process.*, vol. 44, no. 9, pp. 2141–2150, 1996.

[21] H. M. Ozaktas and M. A. Kutay, "The fractional Fourier transform," in *Proc. European Control Conf. (ECC)*, Sep. 2001.

[22] S. I. Ahmed and I. Darwazeh, "IDFT based transmitters for spectrally efficient FDM system," in *Proc. London Commun. Symp.*, Sep. 2011.

[23] H. G. Myung, J. Lim, and D. J. Goodman, "Single carrier FDMA for uplink wireless transmission," *IEEE Veh. Technol. Mag.*, vol. 1, no. 3, pp. 30–38, 2006.

[24] Y. J. D. Kim and J. Bajcsy, "On spectrum broadening of pre-coded faster-than-Nyquist signaling," in *Proc. IEEE VTC-Fall*, Sep. 2010.

[25] A. V. Oppenheim, J. R. Buck, and R. W. Schafer, *Discrete-time signal processing. Vol. 2*. Upper Saddle River, NJ: Prentice Hall, 2001.

[26] D. Rainnie, Y. Feng, and J. Bajcsy, "On capacity merits of spectrally efficient FDM," in *Proc. IEEE MILCOM*, Oct. 2015.

[27] Y. J. D. Kim, "Properties of faster-than-Nyquist channel matrices and folded-spectrum, and their applications," in *Proc. IEEE WCNC*, Apr. 2016.